Superluminal advanced transmission of *X* waves undergoing frustrated total internal reflection: The evanescent fields and the Goos-Hänchen effect

Amr M. Shaarawi*

Physics Department, The American University in Cairo, P.O. Box 2511, Cairo 11511, Egypt

Bassem H. Tawfik

Department of Engineering Physics and Mathematics, Faculty of Engineering, Cairo University (Fayoum Campus), Fayoum, Egypt

Ioannis M. Besieris

The Bradley Department of Electrical and Computer Engineering, Virginia Polytechnic Institute and State University, Blacksburg, Virginia 24061

A study of *X* waves undergoing frustrated total internal reflection at a planar slab is provided. This is achieved by choosing the spectral plane wave components of the incident *X* wave to fall on the upper interface at angles greater than the critical angle. Thus, evanescent fields are generated in the slab and the peak of the field tunneling through the slab appears to be transmitted at a superluminal speed. Furthermore, it is shown that for deep barrier penetration, the peak of the transmitted field emerges from the rear interface of the slab before the incident peak reaches the front interface. To understand this *advanced* transmission of the peak of the pulse, a detailed study of the behavior of the evanescent fields in the barrier region is undertaken. The difference in tunneling behavior between deep and shallow barrier penetrations is shown to be influenced by the sense of the Goos-Hänchen shift.

I. INTRODUCTION

In this work, we study the frustrated total internal reflection of a classical pulse; namely, the *X* wave [1–5]. Such a wave field is a three-dimensional dispersion-free localized pulse that travels in free space without spreading out. The *X* wave is synthesized of a superposition of polychromatic plane wave components having wave vectors restricted to a conic surface [6,7]. One can then choose the apex angle ξ of the spectral conic surface characterizing the *X* wave to be larger than the critical angle. Consequently, the spectral plane wave components of the *X* wave undergo total internal reflection. Following this approach, it has been recently demonstrated that the peaks of *X* waves undergoing frustrated total internal reflection on the upper surface of a planar slab appear to be transmitted at superluminal speeds [8]. Such a behavior is analogous to theoretical results predicted in relation to the transmission of electromagnetic pulses through undersized waveguides [9] and in situations involving the tunneling of photons [10,11]. Several of these theoretical results have been confirmed in recent experiments [12–17]. Similar predictions have been made in connection with frustrated total internal reflection from the front surface of a thin slab [8,18,19] and for pulses propagating through electromagnetic metamaterials [20]. The latter are materials characterized by equivalent permittivities and permeabilities that are smaller than the free space values. The aforementioned superluminal tunneling effect is usually explained as a result

of reshaping of the field transmitted through the tunneling region before it emerges on the rear side of the barrier. The analysis used in Ref. [8] has been extended to the case of *X* waves tunneling through multilayered structures consisting of alternating layers of evanescent and free-propagation regions [21]. The results obtained in Ref. [21] confirm that the traversal times for *X* waves transmitted through multiple barriers separated by propagation-free regions are independent of the length of the barriers as well as the propagation-free regions separating them [22,23]. For such multilayered structures, it has been shown that the peak of the *X* wave appears to be transmitted at a speed much larger than that of light. Furthermore, it has been predicted that, for deep barrier penetration, *advanced* transmission of the peak of the pulse can take place before the incident peak reaches the front surface of the multilayered stack [21].

Although the behavior of the evanescent fields in the barrier region plays an important role in the reshaping of the tunneling pulse, such fields were not studied in Refs. [8] and [21]. These earlier investigations have emphasized the nature of the transmitted pulse when it emerges from the slab. Only the transmitted fields beyond the rear surface of the slab were calculated [8,21]. In this work, we are primarily interested in the behavior of the evanescent fields inside the barrier region. The Goos-Hänchen effect will be used to explain the *advanced* transmission of the peak of the *X* wave and its superluminality [24,25]. Furthermore, the time dependence of the buildup of the evanescent field in the barrier region will be examined. Along similar lines, a recent study of the evanescent fields associated with a Bessel beam tunneling through a planar slab predicted that the speed of the transmission of the field is extremely fast [26]. That prediction was based on phase velocity calculations. In contradistinc-

————————
  *On leave from the Department of Engineering Physics and Mathematics, Faculty of Engineering, Cairo University, Giza 12211, Egypt.

tion, the current study establishes that the ultrafast transmission of the X wave is related to the temporal position of the maximum of the evanescent field. In addition, the approach used in this work highlights several interesting features of the evanescent fields associated with the tunneling pulse.

In an earlier investigation dealing with the reflection and refraction of an acoustic X wave from a planar interface separating two media, an exact closed-form expression for the evanescent field in the lower half-space has been deduced [27]. Along the axis of propagation, the time dependence of the evanescent field shows that the amplitude increases to a maximum, starts decaying until it acquires negative values, goes through a minimum, and finally decays to zero asymptotically. A key attribute of such behavior is that, for all points inside the second medium, the maximum of the evanescent field is attained before the peak of the incident pulse arrives at the interface. Understanding this behavior is crucial for explaining the *advanced* transmission of the peak of a tunneling X wave. This is the case because evanescent fields in a semi-infinite half-space can approximate the fields generated in a slab for situations involving deep barrier penetration. Therefore, the *advanced* formation of the maximum of the evanescent field, at all points along the axis of propagation, alludes to the possibility that the same behavior might be observed for a pulse tunneling through a thick slab (deep barrier penetration). The details of this point are explored in this work, and conditions for deep barrier penetration are established

The plan of this work is as follows: The analysis used to determine the evanescent field in the barrier region is introduced in Sec. II. Furthermore, formulas are provided for calculating the incident and transmitted X waves. In Sec. III, the special case of a semi-infinite half-space is considered and closed-form expressions for the evanescent fields due to an incident electromagnetic X wave are derived. Also, the behavior of the evanescent fields in a semi-infinite half-space and in a finite-width slab is compared. In Sec. IV, the evanescent-antievanescent series approximation of the field inside the slab is examined and several features of its time dependence are elucidated. The Goos-Hänchen effect associated with the X wave field in the slab is discussed in Sec. V. It is shown, specifically, that the sense of the Goos-Hänchen shift determines whether the tunneling pulse undergoes deep- or shallow-barrier penetration. Concluding remarks are made in Sec. VI.

II. THE TOTAL X WAVE FIELDS IN A THREE-LAYER MEDIUM

Consider the case of frustrated total internal reflection of a three-dimensional X wave normally incident on the slab shown in Fig. 1. Regions 1 and 3 have refractive indices equal to n_1 and the refractive index of region 2 is n_2. By choosing the axicon angle ξ_1 of the incident X wave to be larger than the critical angle $\theta_c = \sin^{-1}(n_2/n_1)$, all spectral plane wave components of the X wave will undergo total internal reflection and evanescent fields will be generated in region 2. For propagation along the positive z direction, transverse electric (TE) polarization of the plane wave com-
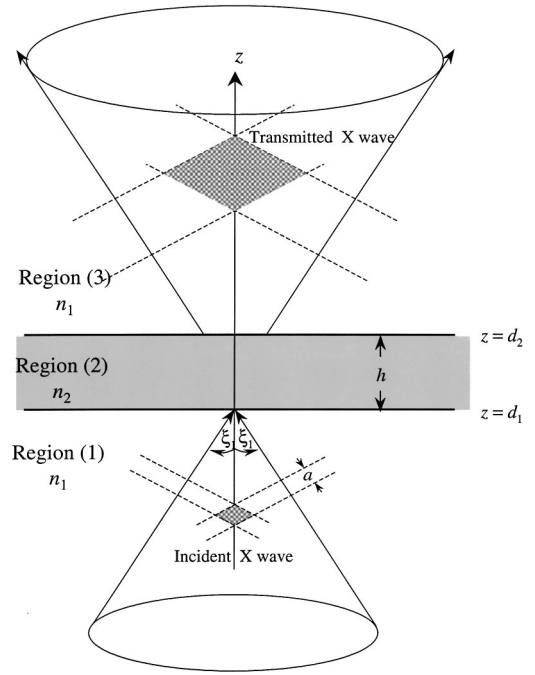

FIG. 1. X wave incident on a slab of width h.

ponent of the X wave is achieved by working with the Hertzian potential

$$\vec{\Pi}_{\mathrm{TE}}(\vec{r},t) = \Psi(\vec{r},t)\vec{u}(z), \qquad (2.1)$$

where $\vec{u}(z)$ denotes a unit vector along the $+z$ direction. The electric field intensity can be readily obtained, viz.,

$$\vec{E}(\vec{r},t) = -Z_0\vec{\nabla}\times\partial_{ct}\vec{\Pi}_{\mathrm{TE}}(\vec{r},t). \qquad (2.2)$$

Here, $Z = \sqrt{\mu_0/\varepsilon}$ and $c = 1/\sqrt{\mu_0\varepsilon}$ assuming that the medium is nonmagnetic. For an X wave normally incident on the slab, the Hertzian potential is defined in terms of a fourfold Fourier superposition as

$$\Psi^{(i)}(\vec{r},t) = \int_{R^1} d(\omega/c_1) \int_{R^3} d^3\vec{k}\hat{A}_1(\vec{k},\omega)e^{-i\omega t}$$
$$\times e^{i(k_x x + k_y y + k_z z)}\delta((\omega/c_1)^2 - k_x^2 - k_y^2 - k_z^2), \qquad (2.3)$$

where $c_1 = c_0/n_1$ is the wave speed in region 1, and c_0 is the speed of light in vacuum. The spectral amplitude of the incident X wave is given by

$$\hat{A}_1(\vec{k},\omega) = \frac{A_1}{\pi}(\omega/\omega_0)^\mu e^{-(\omega/c_1)a}\delta(k_z - (\omega/c_1)\cos\xi_1), \qquad (2.4)$$

where A_1 is a constant amplitude, $a > 0$, and ξ_1 is the axicon angle. The three integrations over $d^3\vec{k}$ are carried out analytically to give

$$\Psi^{(i)}(\vec{r},t)=A_1\int_0^\infty d(\omega/c_1)(\omega/\omega_0)^\mu J_0((\omega/c_1)\rho\sin\xi_1)$$
$$\times e^{-(\omega/c_1)[a-i(z\cos\xi_1-c_1t)]}. \qquad (2.5)$$

For integer values of μ, the integration over (ω/c_1) yields the closed form of the μth order X wave [1,3–5,21]. Using the analysis described in Sec. 2.1 in Ref. [28], we calculate the total field in region 1 by adding a term due to the multiple reflections from the region 2; specifically,

$$\Psi_1(\vec{r},t)=A_1\int_0^\infty d(\omega/c_1)(\omega/\omega_0)^\mu J_0((\omega/c_1)\rho\sin\xi_1)$$
$$\times\{e^{-(\omega/c_1)[a-i(z\cos\xi_1-c_1t)]}$$
$$+\tilde{R}_{12}e^{-(\omega/c_1)[a+i(z\cos\xi_1+c_1t)]}\}. \qquad (2.6)$$

The first term in the integrand represents the incident wave. In the second term, $\tilde{R}_{12}$ is the generalized reflection coefficient for the three-layer medium that relates the backward-traveling and the forward-propagating wave amplitudes in region 1. It includes the effect of rear surface reflection as well as the reflection from the front surface of the slab. This reflection coefficient is given explicitly by [28]

$$\tilde{R}_{12}=R_{12}+\frac{T_{12}R_{23}T_{21}e^{2ik_{2z}(d_2-d_1)}}{1-R_{21}R_{23}e^{2ik_{2z}(d_2-d_1)}}. \qquad (2.7)$$

Here, T_{ij} and R_{ij} are the Fresnel transmission and reflection coefficients at the interface separating regions i and j. For a TE wave incident on an interface separating two electrically different nonmagnetic media, the Fresnel coefficients are equal to

$$R_{ij}^{\text{TE}}=\frac{k_{iz}-k_{jz}}{k_{iz}+k_{jz}}, \qquad (2.8)$$

$$T_{ij}^{\text{TE}}=\frac{2k_{iz}}{k_{iz}+k_{jz}}, \qquad (2.9)$$

where

$$k_{iz}=\sqrt{(\omega/c_i)^2-(\omega/c_1)^2\sin^2\xi_1}=(\omega/c_i)\cos\xi_i,$$
$$i=1,2,3.$$

In analogy to Eq. (2.4), the spectral amplitude in region 2 depends only on k_z and ω. Using the results of Ref. [28], we can associate a Hertzian potential with the field in region 2, viz.,

$$\Psi_2(\vec{r},t)=\pi\int_{R^1}d(\omega/c_1)\int_{R^1}dk_zJ_0(\rho\sqrt{(\omega/c_2)^2-k_z^2})$$
$$\times\hat{A}_2(k_z,\omega)(e^{ik_zz}+\tilde{R}_{23}e^{2ik_zd_2-ik_zz})e^{-i\omega t}. \qquad (2.10)$$

The first term of the integrand represents the forward-propagating wave, while $\tilde{R}_{23}=R_{23}$ in the second term is the

Fresnel reflection coefficient in region 2 due to the reflection by region 3. To ensure the continuity of the amplitude of the field across the interface $z=d_1$, the spectral amplitude in region 2 is chosen as

$$\hat{A}_2(\vec{k},\omega)=\frac{A_2}{\pi}(\omega/\omega_0)^\mu e^{-(\omega/c_1)a}\delta(k_z-(\omega/c_2)\cos\xi_2), \qquad (2.11)$$

where ξ_2 is the apex angle of the spectral cone of the transmitted pulse in the second layer. In the case of total internal reflection, we have

$$\cos\xi_2=i\sqrt{\frac{\sin^2\xi_1}{n_{21}^2}-1}, \quad n_{21}=\frac{n_2}{n_1}=\sqrt{\frac{\varepsilon_2}{\varepsilon_1}}. \qquad (2.12)$$

The amplitude A_2 in the region 2 is related to A_1 through the following expression [28]:

$$A_2=\frac{A_1T_{12}e^{i(k_{1z}-k_{2z})d_1}}{1-R_{21}R_{23}e^{2ik_{2z}(d_2-d_1)}}. \qquad (2.13)$$

In Eq. (2.10), the integration over k_z reduces the total field in region 2 to the form

$$\Psi_2(\vec{r},t)=\int_0^\infty d(\omega/c_1)A_2(\omega/\omega_0)^\mu J_0((\omega/c_1)\rho\sin\xi_1)$$
$$\times\{e^{-(\omega/c_1)(a+z\sqrt{\sin^2\xi_1-n_{21}^2}+ic_1t)}$$
$$+\tilde{R}_{23}e^{-(\omega/c_1)[a-(z-2h)\sqrt{\sin^2\xi_1-n_{21}^2}+ic_1t]}\}, \qquad (2.14)$$

where h is the thickness of the barrier; i.e., $h=d_2-d_1$. Analogously, we can express the field in the third region as

$$\Psi_3(\vec{r},t)=\int_0^\infty d(\omega/c_1)A_3(\omega/\omega_0)^\mu J_0((\omega/c_1)\rho\sin\xi_1)$$
$$\times e^{-(\omega/c_1)(a-i(z\cos\xi_1-c_1t))}, \qquad (2.15)$$

where A_3 is given by [28,8]

$$A_3=\frac{A_1T_{23}T_{12}e^{i(k_{1z}-k_{2z})d_1}e^{i(k_{2z}-k_{3z})d_2}}{1-R_{21}R_{23}e^{2ik_{2z}(d_2-d_1)}}$$
$$=\frac{iA_12Kk_{1z}}{(k_{1z}^2-K^2)\sinh(Kh)+i2Kk_{1z}\cosh(Kh)}. \qquad (2.16)$$

Here, $K=(\omega/c_1)\sqrt{\sin^2\xi_1-n_{21}^2}$ and $k_{1z}=(\omega/c_1)\cos\xi_1$. To illustrate the possibility of advanced transmission of the peak of the X wave, consider an X wave normally incident on a planar slab of refractive index $n_2=1$, while the two surrounding media have refractive indices $n_1=n_3=3$. We choose an X wave of apex angle $\xi_1=85°$ and parameter a $=0.2$ mm. Note that $\xi_1\gg\sin^{-1}n_{21}=19.47°$; therefore, all spectral plane wave components of the X wave undergo frustrated total internal reflection at the front interface. The total field in all three layers is displayed in Fig. 2 for $\mu=0$. The
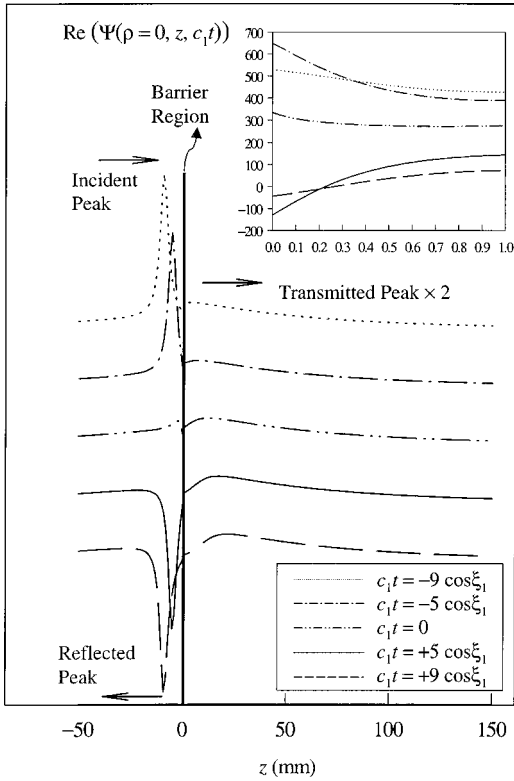
FIG. 2. Advanced transmission of the axial profile of the Hertzian potential of an X wave incident on a slab of width $h=1$ mm. The refractive indices of the three regions are equal to $n_2=1$ and $n_1=n_3=3$. The incident X wave is characterized by $\xi_1=85°$, $a=0.2$ mm, and $\mu=0$. The total fields are plotted at $c_1t=-9\cos\xi_1$, $c_1t=-5\cos\xi_1$, $c_1t=0$, $c_1t=+5\cos\xi_1$, and $c_1t=+9\cos\xi_1$ mm. The amplitude of the transmitted field is multiplied by a factor of 2 to emphasize the shape of the peak in region 3. The insets show enlargements of the Hertzian potential associated with the evanescent field at different times.

width of the barrier region is chosen to equal $h=1$ mm. The fields are plotted at five different times, $c_1t=-9\cos\xi_1$, $-5\cos\xi_1$, 0, $+5\cos\xi_1$, and $+9\cos\xi_1$ mm. At time $c_1t=-9\cos\xi_1$ mm, the peak of the transmitted field, shown magnified by a factor of 2, has already emerged from the rear surface of the slab. The evanescent fields inside the barrier region are displayed in the insets included in the figure. The plots show clearly that for deep barrier penetration, the peak of the transmitted pulse appears on the rear side of the barrier before the incident peak reaches the front interface. This behavior does not exist for small axicon angles, i.e., when ξ_1 is slightly larger than the critical angle [8]. It should be noted that the insets show that the evanescent field displays a continuous decay in amplitude as one moves from the front to the rear interface. For $c_1t>-9\cos\xi_1$ mm, the amplitude of the evanescent field at $z=1$ mm falls constantly with time. This indicates that the peak is transmitted into region 3. In contrast, the initial increase in the amplitude of the evanescent field at the front interface $(z=0)$, followed by a negative flip, is a sign of the arrival of the incident pulse and its subsequent reflection. Consequently, the time at which the evanescent field attains its maximum amplitude can be used
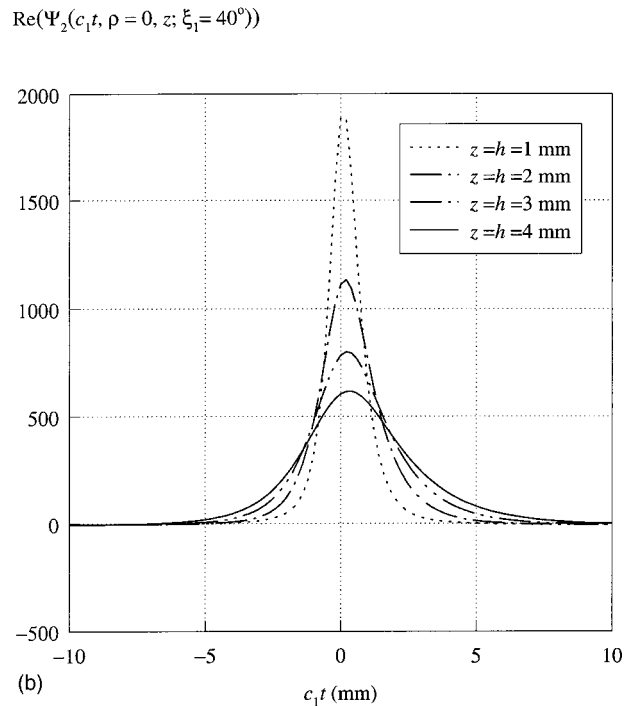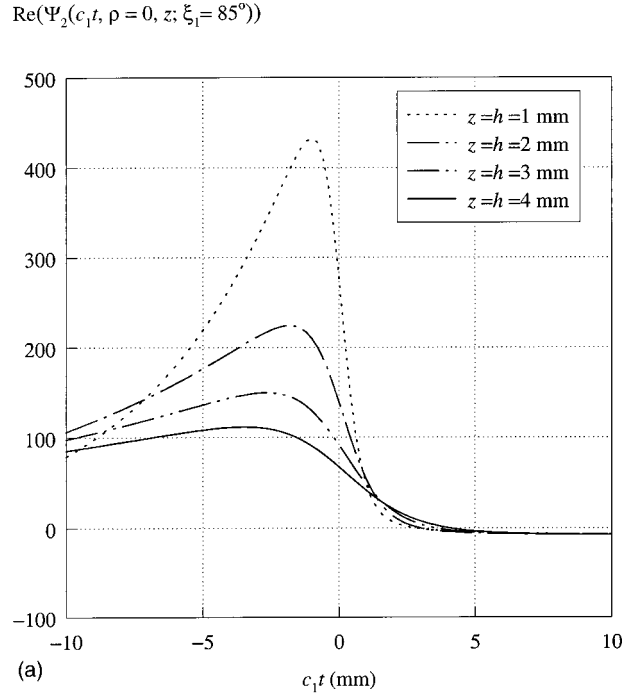

FIG. 3. The time dependence of the Hertzian potential associated with the evanescent field at the rear surfaces of slabs having different widths. The incident X wave and the planar slab are the same as in Fig. 2. The apex angle of the X wave equals (a) $\xi_1=85°$ and (b) $\xi_1=40°$.

to predict when the peak of the transmitted pulse emerges from the barrier region and to determine when does *advanced* transmission occur.

In Fig. 3(a), the time dependence of the Hertzian potential associated with the evanescent field is shown at the rear interface of various slabs having different widths, i.e., at z

$=h$. One should note that for all widths the evanescent fields attain their maximum amplitudes at negative times, i.e., at times prior to the arrival of the peak of the incident pulse at the front interface. This behavior determines the condition for deep barrier penetration, viz., $\xi_1 \gg \sin^{-1} n_{21}$. To appreciate the importance of such a condition for attaining deep barrier penetration, we have calculated the time dependence of the evanescent field for $\xi_1 = 40°$. The Hertzian potentials associated with the resulting evanescent fields are shown in Fig. 3(b). For the chosen barrier widths, the maxima of the evanescent fields occur at positive values of time. This means that, for $\xi_1 = 40°$, the peak of the transmitted field will appear after the incident peak reaches the front interface and no *advanced* transmission takes place. Nevertheless, the peak of the pulse is transmitted at a superluminal speed because the peak arrival time $(c_1/\cos \xi_1)t_p < h$ for the four barrier widths considered in Fig. 3(c).

III. THE EVANESCENT X WAVES

Consider the case of an electromagnetic X wave normally incident on a planar surface of discontinuity separating two different media with refractive indices n_1 and n_2, respectively. Assume that the interface separating the two media is situated at $z=0$. Choosing $n_1 > n_2$, the spectral plane wave components of the X wave will undergo total internal reflections and evanescent fields will be generated in region 2. The Hertzian potential associated with the transmitted field can be derived directly from Eq. (2.15) after removing the term responsible for the reflection from the rear interface ($R_{23} = 0$), specifically,

$$\Psi_{\text{tran}}(\vec{r},t) = \int_0^\infty d(\omega/c_1) A_1 T_{12} J_0((\omega/c_1)\rho \sin \xi_1)$$

$$\times e^{-(\omega/c_1)(a+z\sqrt{\sin^2 \xi_1 - n_{21}^2}+ic_1 t)}. \quad (3.1)$$

Here, the Fresnel transmission coefficient, which is expressed explicitly as

$$T_{12} = \frac{2k_{1z}}{k_{1z}+k_{2z}} = \frac{2(\omega/c_1)\cos \xi_1}{(\omega/c_1)\cos \xi_1 + (\omega/c_2)\cos \xi_2}$$

$$= \frac{2 \cos \xi_1}{\cos \xi_1 + i\sqrt{\sin^2 \xi_1 - n_{21}^2}}, \quad (3.2)$$

does not depend on ω. Consequently, the integration in Eq. (3.1) can be evaluated using formula (6.611) in Ref. [29], yielding the closed-form expression

$$\Psi_{\text{tran}}(\vec{r},t) = \frac{2A_1 \cos \xi_1}{(\cos \xi_1 + i\Gamma)\sqrt{\rho^2 \sin^2 \xi_1 + (a+z\Gamma+ic_1 t)^2}}, \quad (3.3)$$

where $\Gamma = \sqrt{\sin^2 \xi_1 - n_{21}^2}$. This evanescent field exhibits a transverse wave motion along the interface through the term $\rho^2 \sin^2 \xi_1 - (c_1 t)^2$ appearing in the square root in the denomi-
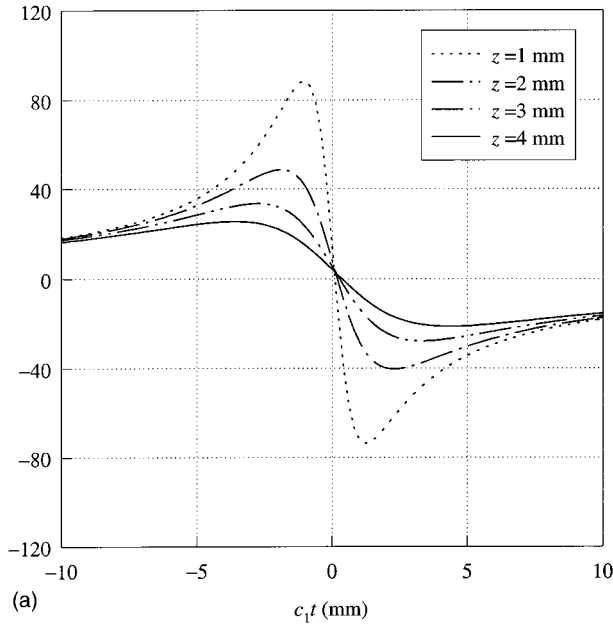
nator. As for the axial time evolution of the evanescent field, consider the real part of the expression given in Eq. (3.3) for $\rho = 0$, specifically,

$$\text{Re}\{\Psi_{\text{tran}}(\rho = 0, z, t)\}$$

$$= \frac{2A_1[a \cos^2 \xi_1 + \Gamma \cos \xi_1(z \cos \xi_1 - c_1 t)]}{[(c_1 t)^2 + (a+z\Gamma)^2](1 - n_{21}^2)}. \quad (3.4)$$

This function has a null that propagates at a speed equal to $c_1/\cos \xi_1$. In Fig. 4(a), the time dependence of the Hertzian potential associated with the evanescent field is shown for the semi-infinite half-space at different depths z from the interface. One should note that for all distances from the interface the evanescent fields attain their maximum amplitudes at negative times, i.e., at times prior to the arrival of the peak of the incident pulse at the front interface. The shapes of the Hertzian potentials shown in Fig. 3(a) differ from those shown in Fig. 4(a) because of the effect of the antievanescent components reflected from the back interface of the finite-width slab. It appears from Figs. 3(a) and 4(a) that the reflection from the interface separating regions 2 and 3 affects primarily the trailing edge of the field. On the other hand, the time dependence around the rising edge and the field's maximum has the same shape in both cases considered in Figs. 3(a) and 4(a). The crucial point, here, is that the maximum amplitudes of the evanescent fields are attained at negative times. For $\xi_1 = 40°$, the Hertzian potentials associated with the evanescent fields are shown in Fig. 4(b). Unlike the evanescent fields associated with the finite-width slab [cf. Fig. 3(b)], one should note that for the semi-infinite half-space all maxima are attained at negative times.

To establish the conditions leading to *advanced* transmission, we have calculated the axial time dependence of the evanescent field at different points inside a slab of width $h = 4$ mm. Figure 5(b) shows the time dependence of the evanescent field for $\xi_1 = 85°$ at distances $z = 1, 2, 3,$ and 4 mm. Apart from expected differences in amplitudes, one should note the similarity between the temporal profiles of these plots and the ones provided in Fig. 4(a). A striking feature that should be pointed out is the peaking of the evanescent field at deeper distances inside the slab before occurring at distances closer to the front interface. This behavior, which is an attribute of evanescent fields formed in a semi-infinite half-space, is the reason for *advanced* transmission. In Fig. 5(b), the time dependence of the evanescent field associated with an incident X wave having $\xi_1 = 40°$ is plotted at different distances inside a slab of width 4 mm. It is interesting to note that, similar to the semi-infinite half-space, the evanescent field peaks at negative times for $z = 1, 2,$ and 3 mm. This behavior is expected to take place when the barrier is wide enough to be approximated by a semi-infinite half-space. However, at the rear surface of the slab ($z = h = 4$ mm) the maximum amplitude is achieved at a positive time. Furthermore, in contrast with the $\xi_1 = 85°$ case, the peaking of the evanescent field occurs first at distances closer to the front

$Re(\Psi_{tran}(c_1 t, \rho = 0, z; \xi_1 = 85^o))$

$Re(\Psi_2(c_1 t, \rho = 0, z; \xi_1 = 85^o))$

$Re(\Psi_{tran}(c_1 t, \rho = 0, z; \xi_1 = 40^o))$

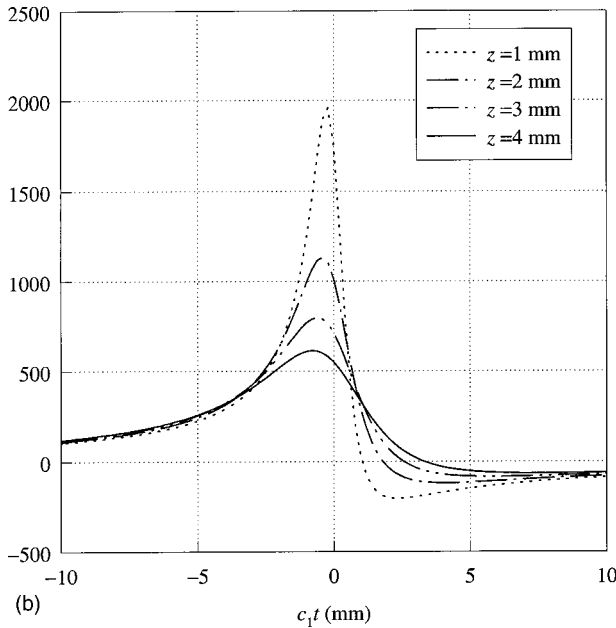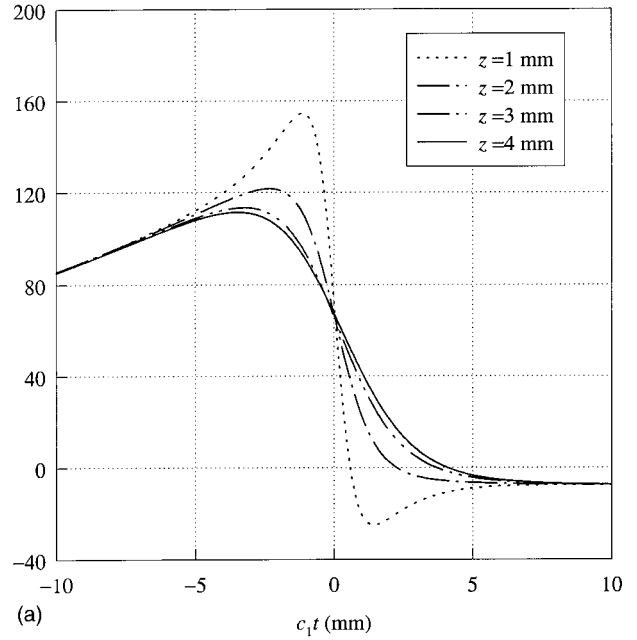$Re(\Psi_2(c_1 t, \rho = 0, z; \xi_1 = 40^o))$

FIG. 4. Same as Fig. 3 but for an X wave incident on a semi-infinite half-space. The time dependences are calculated at different distances from the interface separating two regions having refractive indices $n_1 = 3$ and $n_2 = 1$. The apex angle of the X wave equals (a) $\xi_1 = 85°$ and (b) $\xi_1 = 40°$.
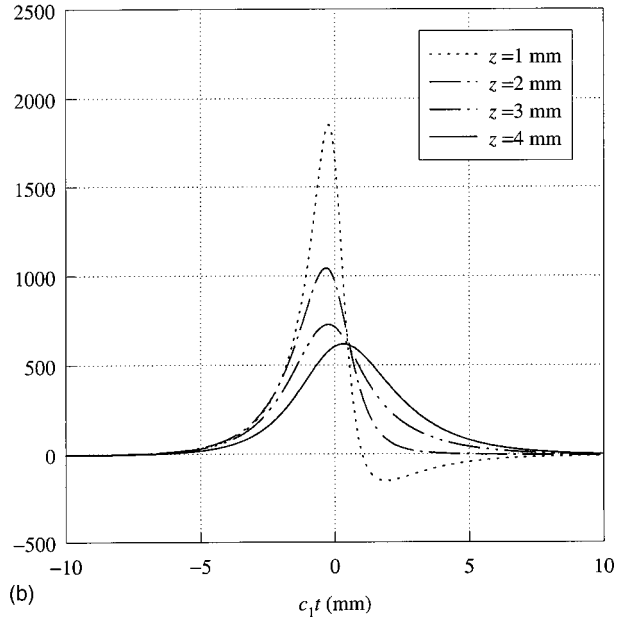
FIG. 5. Same as Fig. 3 but for an X wave incident on a slab of width $h = 4$ mm. The time dependences are calculated at different distances from the interface. The refractive indices of the three regions are $n_1 = n_3 = 3$ and $n_2 = 1$. The apex angle of the X wave equals (a) $\xi_1 = 85°$ and (b) $\xi_1 = 40°$.

interface and moves forward towards the rear surface of the barrier.

In a study of the tunneling of Bessel beams, it has been predicted that, immediately after the front interface of the slab, the wave motion is extremely fast when compared to the wave speed at the rear surface, i.e., at $z = h$ [26]. For X

waves having $\xi_1 = 40°$, negative-time *advanced* formation of the peak of the evanescent field takes place over most of the slab, except for a small region close to the rear interface. This result agrees in essence with the predictions made in Ref. [26]; namely, that wave transmission through an evanes-

cent channel is initially very fast over most of the slab until the antievanescent components become significant close to the rear surface. However, *advanced* peaking of the evanescent field within the slab was not discussed *per se* in the aforementioned reference. Such a phenomenon reflects the extraordinary speed of peak transmission of X waves through the evanescent channel. This behavior was not captured by the phase (or group) velocity analysis used in Ref. [26] for continuous wave Bessel beams. For large ξ_1 angles, *advanced* peaking of the evanescent field of an X wave extends over the whole slab with the field peaking first at the rear interface. As such, the peak of the evanescent field appears to be anomalously moving backwards with time from the rear to the front surface of the slab. The two situations considered in Figs. 5(a) and 5(b) show distinct behaviors as far as the peaking times are concerned. For $\xi_1 = 85°$, the peaking times are negative for all distances from the front interface, and there is a negative shift in the temporal position of the peaks as z increases, i.e., the peak of the evanescent field appears to be moving backwards. As for $\xi_1 = 40°$, forward motion of the peak takes place. Figure 5(b) shows that the peaking time of the evanescent field occurs initially at a negative time; henceforth, it exhibits positive shifting with distance until it acquires maximum amplitude at a positive $c_1 t_p$ value at the surface $z = h$.

The preceding discussion indicates that the time at which the evanescent fields acquire their maxima determines if *advanced* transmission will take place. To clarify this point, we have calculated the dependence of the peaking time $c_1 t_p$ of the evanescent field on the axicon angle ξ_1. From the discussion in the preceding section, we expect that for an intermediate value $40° < \xi_1 < 85°$, a zero peaking time at $z = h$ will occur. This is confirmed in Fig. 6(a) that displays the peaking time as a function of ξ_1 at the rear edge of the slab for different barrier widths. It is interesting to note that $c_1 t_p$ acquires negative values for $\xi_1 > 48.19°$ independently of the barrier width. The same result holds even when the barrier width is increased to the relatively large value $z = h = 1$ m. This suggests that deep barrier penetration depends only on the axicon angle, i.e., transmission through a thick barrier is not sufficient to cause the *advanced* tunneling of the peak of a X wave. Furthermore, one can show that the peaking time is also independent of the value of the parameter a characterizing the incident X wave. To establish this point, plots of the peaking time for different a values are provided in Fig. 6(b).

IV. THE EVANESCENT-ANTIEVANESCENT SERIES APPROXIMATION

To be able to differentiate between deep and shallow barrier penetration, we have to determine why the peaking time changes from positive values for small ξ_1 angles to negative values for $\xi_1 > 48.19°$. One also has to figure out what is so special about the angle for $\xi_1 = \xi_1^{(0)} = 48.19°$ corresponding to zero-tunneling time. Specifically, why is it independent of both the width of the barrier and the parameter a? Along such direction, we examine an approximation of Eq. (2.14) that involves the first order evanescent-antievanescent com-
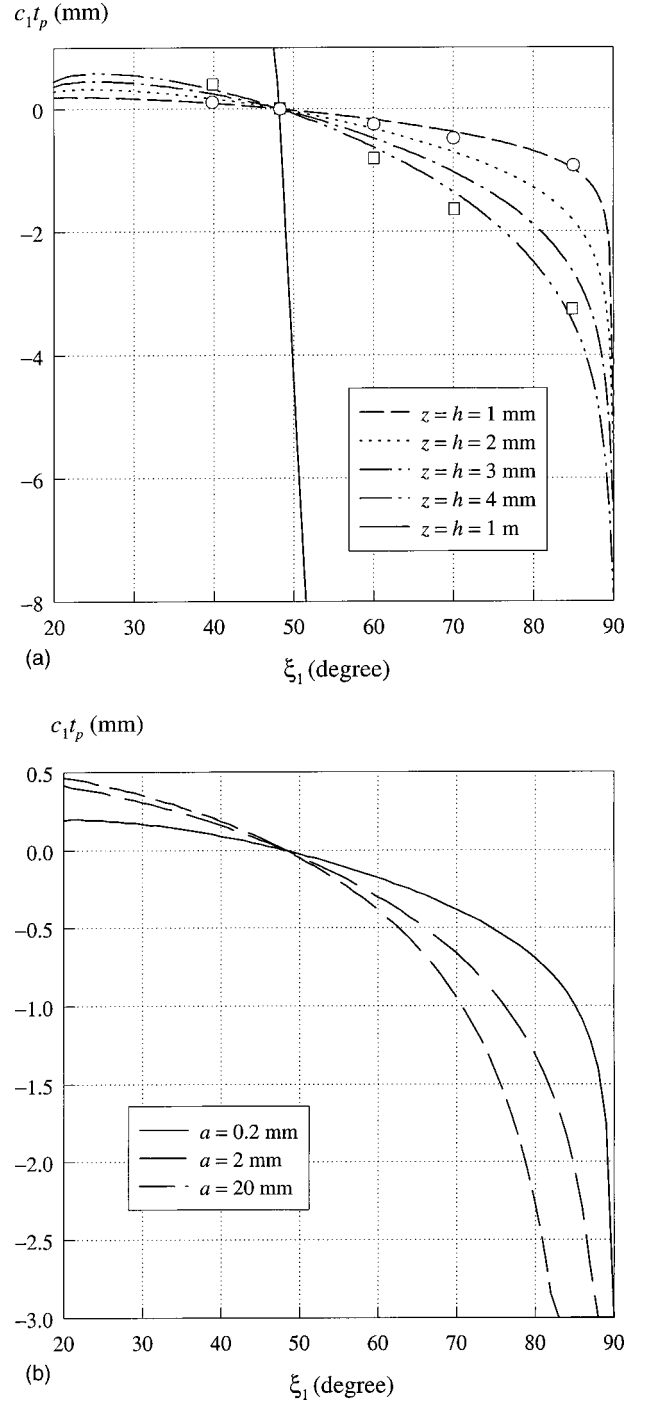

FIG. 6. Peaking time $c_1 t_p$ vs ξ_1 for different (a) slab widths h and (b) parameter a values. The circles and squares represent sample points calculated using Eq. (4.6) for $h = 1$ and 4 mm, respectively.

ponents. This is done by expressing the amplitude given in Eq. (2.13) in terms of a series expansion, viz.,

$$A_2 = A_1 T_{12} e^{i(k_{1z} - k_{2z})d_1} \{ 1 + R_{21} R_{23} e^{2ik_{2z}(d_2 - d_1)} + R_{21}^2 R_{23}^2 e^{4ik_{2z}(d_2 - d_1)} + \cdots \}. \tag{4.1}$$

Retaining only the first term, Eq. (2.14) acquires the following form:

$$\Psi_2^{(1)}(\vec{r},t) = \int_0^\infty d(\omega/c_1) A_1 T_{12} e^{i(k_{1z}-k_{2z})d_1}(\omega/\omega_0)^\mu J_0((\omega/c_1)\rho \sin \xi_1)\{e^{-(\omega/c_1)(a+z\sqrt{\sin \xi_1-n_{21}^2}+ic_1t)}$$

$$+ \tilde{R}_{23} e^{-(\omega/c_1)[a-(z-2h)\sqrt{\sin^2 \xi_1-n_{21}^2}+ic_1t]}\}. \tag{4.2}$$

$\Psi_2^{(1)}(\vec{r},t)$ is the first order approximation of $\Psi_2(\vec{r},t)$ when only the first term in the series given in Eq. (4.1) is retained. Physically, this approximation is equivalent to working only with the first order evanescent and the antievanescent fields. All other higher order pairs arising due to successive reflections are neglected. Although this approximation may not be accurate for all parameter values of interest, working with the first order of evanescent-antievanescent pair clarifies several aspects of *advanced* peak transmission.

The integration given in Eq. (4.2) can be carried out to give a sum of two terms analogous to the one given in Eq. (3.3) for a semi-infinite half-space. Specifically, for $\mu=0$, the approximate Hertzian potential along the axis of propagation is given as

$$\Psi_2^{(1)}(\rho=0,z,t) = \frac{2A_1 \cos \xi_1}{(\cos \xi_1 + i\Gamma)(a+z\Gamma+ic_1t)}$$
$$- \frac{2A_1 \cos \xi_1(\cos \xi_1 - i\Gamma)}{(\cos \xi_1 + i\Gamma)^2[a-(z-2h)\Gamma+ic_1t]}. \tag{4.3}$$

Rearranging terms, the real part of the above expression becomes equal to

$$\text{Re}\{\Psi_2^{(1)}(\rho=0,z,t)\}$$
$$= \frac{2A_1 \cos^2 \xi_1}{(1-n_{21}^2)^2}\left\{\frac{(1-n_{21}^2)[a+\Gamma(z-v_et)]}{(c_1t)^2+(a+z\Gamma)^2}\right.$$
$$\left.+ \frac{(\cos^2 \xi_1 - 3\Gamma^2)[-(a+2h\Gamma)+\Gamma(z+v_at)]}{(c_1t)^2+[a-(z-2h)\Gamma]^2}\right\}, \tag{4.4}$$

where the velocities of the evanescent and antievanescent nulls, denoted by v_e and v_a, are given by

$$v_e = \frac{c_1}{\cos \xi_1}, \tag{4.5a}$$

$$v_a = -\frac{(3\cos^2 \xi_1 - \Gamma^2)}{\Gamma(\cos^2 \xi_1 - 3\Gamma^2)}\frac{c_1}{\cos \xi_1}. \tag{4.5b}$$

The peak of the time dependence of the evanescent field at the rear edge of the barrier region ($z=h$) can be deduced by equating the time derivative of Eq. (4.4) to zero. This procedure yields the following expression for the peaking time:

$$c_1t_p = (a+z\Gamma)\frac{(\cos \xi_1 - \Gamma)}{(\cos \xi_1 + \Gamma)}. \tag{4.6}$$

Sampled values of c_1t_p calculated using Eq. (4.6) are shown in Fig. 6(a). The zero-tunneling-time angle $\xi_1^{(0)}$ can be calculated by setting $c_1t_p=0$ in Eq. (4.6), thus, obtaining

$$\cos \xi_1^{(0)} = \sqrt{\frac{1-n_{21}^2}{2}}, \tag{4.7}$$

which is independent of both h and a, as anticipated by the plots shown in Figs. 6(a) and 6(b). For $n_{21}=\frac{1}{3}$, Eq. (4.7) yields $\xi_1^{(0)}=48.19°$ as predicted by Figs. 6(a) and 6(b). The expression for the angle $\xi_1^{(0)}$ given in Eq. (4.7) could also be obtained upon setting $v_e=v_a$. Although the expression given in Eq. (4.7) is derived within the limits of the first order evanescent-antievanescent approximation, we claim that it can be used as a condition for deep barrier penetration of an X wave tunneling through a planar slab. This claim is valid because all higher order pairs satisfy the same condition. To improve this first order approximation, we can include higher order pairs. Using the series expansion given in Eq. (4.1), we obtain the following expression for the time dependence of the evanescent fields at the rear edge of the barrier region:

$$\Psi_2(\rho=0,z=h,t)$$
$$= \frac{4A_1\Gamma \cot \xi_1}{(1-n_{21}^2)}\sum_{\ell=1}^\infty \frac{\exp(-i\Phi_\ell)}{[a+(2\ell-1)h\Gamma+ic_1t]}. \tag{4.8a}$$

Here,

$$\Phi_\ell = (4\ell-2)\tan^{-1}(\Gamma/\cos \xi_1) + (\pi/2). \tag{4.8b}$$

This is a particularly simple expression describing the time dependence of the evanescent field at the rear surface of the barrier. The summation in Eq. (4.8) is over terms representing the time variations of all multiply reflected evanescent-antievanescent pairs. Apart from the phase factor, the individual terms have simple time dependence analogous to that of the half-space evanescent field. The $(2\ell-1)h\Gamma$ term in the denominator of each term represents the different distances traversed by the ℓth order evanescent-antievanescent pairs after undergoing multiple reflections at the front and rear interfaces of the barrier. This factor is also responsible for reducing the amplitudes of the higher order terms and increasing their temporal spread.

Notice that all terms in the series given in Eq. (4.8) peak at $c_1t=0$ when the following condition is satisfied:

$$\Phi_\ell \equiv (4\ell-2)\tan^{-1}(\Gamma/\cos \xi_1) + (\pi/2) = \ell\pi. \tag{4.9}$$

After some manipulation, it can be shown that Eq. (4.9) reduces to the same condition given in Eq. (4.7). The evanescent field on the rear interface peaks at $c_1 t_p = 0$ when $\xi_1 = \xi_1^{(0)} = 48.19°$. This condition applies separately to each evanescent-antievanescent pair in the series (4.8).

V. THE GOOS-HÄNCHEN SHIFT AND ADVANCED TRANSMISSION

It has been recently pointed out that the Goos-Hänchen shift causes the superluminal transmission of pulses in situations involving frustrated total internal reflection at a double prism [24,25]. In this section, we apply a similar procedure to the pulsed plane wave representation of X waves [3,30] in order to understand how the transmitted peak is formed. We demonstrate that, besides being responsible for the superluminality of the transmission, the Goos-Hänchen shift accounts for the difference between deep and shallow barrier penetrations.

It is well established that the X wave solutions can be synthesized as a superposition over Bessel beams [30]. Additionally, it has been recently shown that an X wave can be represented as an angular superposition of pulsed fields traveling at a tilted angle ξ_1 with respect to the axis of propagation of the peak of the X wave [3,30]. This view leads to a wave representation in the form of a superposition of tilted pulsed fields, viz.,

$$\Psi(x,y,z) = \int_0^{2\pi} d\phi F(\phi) g^+[c_1 t - z \cos \xi_1 - (x \cos \phi + y \sin \phi) \sin \xi_1], \quad (5.1a)$$

over the azimuthal angle ϕ in the plane normal to the direction of propagation of the synthesized pulse [30]. Here,

$$g^+(\zeta) = \frac{1}{\pi} \int_0^\infty d(\omega/c_1) e^{i(\omega/c_1)\zeta} G(\omega/c_1), \quad \text{Im}(\zeta) > 0 \quad (5.1b)$$

is a complex analytic signal, with $\zeta = c_1 t - z \cos \xi_1 - (x \cos \phi + y \sin \phi) \sin \xi_1$. For the case of axisymmetric X wave solutions, we have $F(\phi) = 1$. The incident and transmitted X waves, considered in Sec. II, have the spectra $G_{\text{inc}}(\omega) = (A_1/2)(\omega/\omega_0)^\mu e^{-(\omega/c_1)a}$, and $G_{\text{tran}}(\omega) = (A_3/2) \times (\omega/\omega_0)^\mu e^{-(\omega/c_1)a}$, respectively. The azimuthal superposition given in Eq. (5.1) can be used to calculate the Goos-Hänchen shift for all pulsed field components. In particular, the Goos-Hänchen shift D can be calculated by evaluating the derivative of the phase shift exhibited by the azimuthally pulsed fields transmitted into region 3. Specifically, we need to evaluate [24]

$$D = -\frac{\partial \Phi}{\partial \chi}, \quad (5.2a)$$

where $\chi = (\omega/c_1) \sin \xi_1$ is the wave vector component parallel to the interface. The phase shift Φ of the various spectral

amplitudes of the azimuthal pulsed components is deduced from Eq. (2.16), viz.,

$$\Phi = \arctan\left\{ \frac{\cos^2 \xi_1 - \Gamma^2}{2\Gamma \cos \xi_1} \tanh(Kh) \right\}. \quad (5.2b)$$

The derivative in Eq. (5.2a) yields

$$D = -\frac{2d\Gamma^2 \cot \xi_1 (\cos^2 \xi_1 - \Gamma^2)}{\cosh^2(Kh)\{(2\Gamma \cos \xi_1)^2 + [(\cos^2 \xi_1 - \Gamma^2)\tanh(Kh)]^2\}}. \quad (5.3)$$

No terms in this expression for the Goos-Hänchen shift can acquire negative values except the quantity $(\cos^2 \xi_1 - \Gamma^2)$ in the numerator. Consequently, the Goos-Hänchen shift alters its sign depending on whether

$$\cos^2 \xi_1 - \Gamma^2 > 0 \Rightarrow \text{Negative shift}$$

or

$$\cos^2 \xi_1 - \Gamma^2 < 0 \Rightarrow \text{Positive shift}.$$

The borderline condition, $\cos^2 \xi_1^{(0)} = \Gamma^2 = \sin^2 \xi_1^{(0)} - n_{21}^2$, leads directly to the result given in Eq. (4.7).

In order to understand the reason that the sense of the Goos-Hänchen shift leads to the condition given in Eq. (4.7), we introduce in Fig. 7 a schematic representation of X waves that clarifies their *advanced* tunneling. We have previously shown that X waves can be synthesized of pulsed waves traveling along the propagation vectors lying on a circular cone [3,30]. In the case under consideration, the half apex angle of the cone is equal to ξ_1. This is illustrated in Fig. 7(a) where only two propagation vectors are shown in a vertical section of the conic surface. The peak of the X wave is formed at the intersection of the pulsed wave components. In region 1, two intersecting pulsed waves (W_{1i}, W'_{1i}) and (W_{2i}, W'_{2i}) are sketched at different times t_1 and t_2. In the sketch, we have chosen t_2 to be the time at which the transmitted pulse appears at the rear interface of the barrier region. The evanescent fields associated with the obliquely incident plane wave components are represented by (W_{1e}, W'_{1e}) and (W_{2e}, W'_{2e}). The transmitted pulsed plane wave components are indicated by (W_{1t}, W'_{1t}) and (W_{2t}, W'_{2t}). The negative and positive Goos-Hänchen shifts are illustrated in Figs. 7(a) and 7(b), respectively. In both figures, we have assumed that the time taken by the evanescent fields to tunnel through the barrier is much smaller than the propagation times in regions 1 and 3 [25]. For the negative Goos-Hänchen shift (when $\xi_1 < \xi_1^{(0)}$), the intersection of the incident pulsed plane waves at t_2 is well beyond the front surface of the barrier slab. This indicates that the incident pulse has already passed the front interface before the transmitted pulse exits the barrier region. The intersection of the dashed pulsed plane waves inside region 2 specifies the position of the peak of the X wave traveling in free space. The X wave pulse transmitted into region 3 is shown to be slightly ahead of the free-space one. However, there is no *advanced* transmission in this case because the transmitted pulse exits the barrier region after the peak of the incident
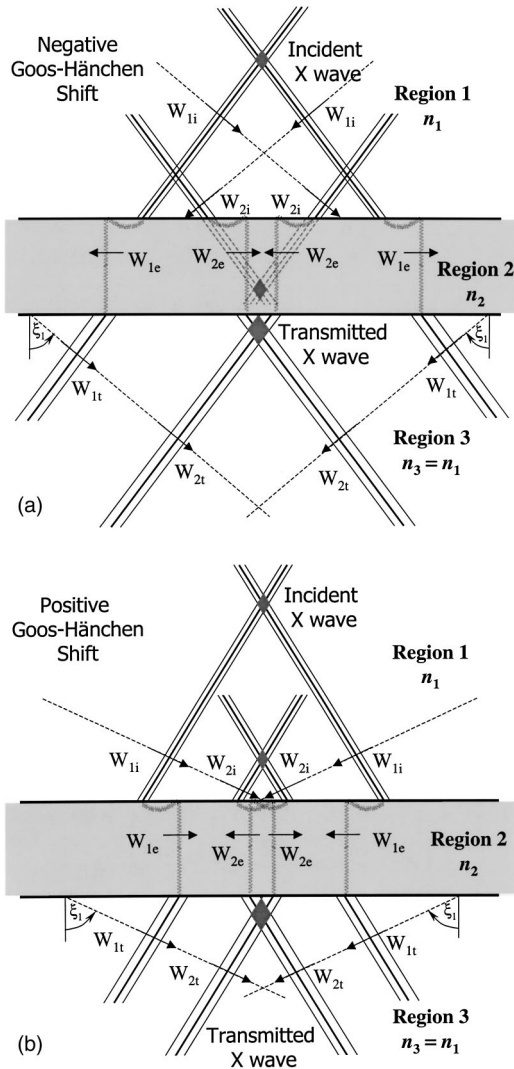
FIG. 7. Ultrafast transmission of the peak of an X wave pulse exhibiting (a) negative and (b) positive Goos-Hänchen shifts.

pulse has passed through the front interface of region 2. In contradistinction, Fig. 7(b) shows that for the positive Goos-Hänchen shift (when $\xi_1 > \xi_1^{(0)}$) the transmitted pulse at t_2 emerges from the rear side of the barrier before the incident pulse reaches the front surface.

VI. CONCLUDING REMARKS

We have established that X waves tunneling through a planar slab can produce *advanced* transmission. Specifically, that the peak of the transmitted pulse emerges from the barrier before the incident peak reaches the front surface. This

behavior is due to classical wave transmission through evanescent channels. It has been argued that in this respect X waves fall in the same category as plane waves going through resonant media, or undersized waveguides [31]. This kind of behavior cannot violate special relativity in a global sense, because the transmitted peak is formed inside the leading portion of the extended field structure of the X wave. Moreover, the wave front of the X wave propagates at the speed of light [31–33]. The point that we would like to stress here is that the ultrafast transmission of the peak is a nonfictitious effect and is accompanied by an observable transfer of the electromagnetic energy surrounding the peak. Whether or not such peaks can carry signals is a matter of debate [31–36].

A crucial point in our analysis is that for an X wave incident on a semi-infinite half-space, the evanescent field at all axial points inside the barrier becomes maximum before the incident peak reaches the interface separating the two electrically different media. Thus, one expects a similar behavior to be observed for an X wave tunneling through a barrier of large width. However, it is established in Sec. IV that *advanced* transmission of a tunneling X wave is independent of the width of the barrier, but depends on the axicon angle of the X wave and the refractive indices of the various regions. The condition given in Eq. (4.7) can thus be used to differentiate between deep and shallow barrier penetrations for which $\xi_1 > \xi_1^{(0)}$ and $\xi_1 < \xi_1^{(0)}$, respectively. We have also established that the Goos-Hänchen shift plays a crucial role in the ultrafast transmission of the peak of the pulse through the barrier region. In particular, we have shown that the sense of the Goos-Hänchen shift determines whether the tunneling X wave will undergo deep or shallow barrier penetration. Consequently, this condition decides whether advanced transmission of the peak takes place or not.

For deep barrier penetration $(\xi_1 > \xi_1^{(0)})$, the *advanced* peaking of the evanescent field of an X wave extends over the whole slab, with the field peaking first at the rear interface. Subsequently, the peak of the evanescent field appears to be anomalously moving backwards with time from the rear to the front surface of the slab. This unusual behavior is similar to negative group velocities associated with light propagation in media exhibiting anomalous dispersion [37–39]. The interesting point here is that the slab through which the X wave is tunneling is nondispersive. The backward motion of the peak of the evanescent field of an X wave is purely an interference effect.

[1] J. Y. Lu and J. F. Greenleaf, IEEE Trans. Ultrason. Ferroelectr. Freq. Control **39**, 19 (1992).

[2] R. W. Ziolkowski, I. M. Besieris, and A. M. Shaarawi, J. Opt. Soc. Am. A **10**, 75 (1993).

[3] P. Saari and K. Reivelt, Phys. Rev. Lett. **79**, 4135 (1997).

[4] I. M. Besieris, M. Abdel-Rahman, A. Shaarawi, and A. Chatzipetros, Prog. Electromagn. Res. **19**, 1 (1998).

[5] E. Recami, Physica A **252**, 586 (1998).

[6] J. Fagerholm, A. T. Friberg, J. Huttunen, D. P. Morgan, and M. M. Salomaa, Phys. Rev. E **54**, 4347 (1996).

[7] A. T. Friberg, J. Fagerholm, and M. M. Salomaa, Opt. Commun. **136**, 207 (1997).

[8] A. M. Shaarawi and I. M. Besieris, Phys. Rev. E **62**, 7415 (2000).

[9] T. Emig, Phys. Rev. E **54**, 5780 (1996).

[10] J. Jakiel, V. S. Olkhovsky, and E. Recami, Phys. Lett. A **248**, 156 (1998).

[11] Th. Martin and R. Landauer, Phys. Rev. A **45**, 2611 (1992).

[12] G. Nimtz, A. Enders, and H. Spieker, J. Phys. I **4**, 1 (1994).

[13] A. Enders and G. Nimtz, J. Phys. I **2**, 1693 (1992).

[14] A. Enders and G. Nimtz, Phys. Rev. E **48**, 632 (1993).

[15] D. Mugnai, A. Ranfagni, R. Ruggeri, A. Agresti, and E. Recami, Phys. Lett. A **209**, 227 (1995).

[16] A. M. Steinberg, P. G. Kwiat, and R. Y. Chiao, Phys. Rev. Lett. **71**, 708 (1993).

[17] V. Laude and P. Tournois, J. Opt. Soc. Am. B **16**, 194 (1999).

[18] Ph. Balcou and L. Dutriaux, Phys. Rev. Lett. **78**, 851 (1997).

[19] J. J. Carey, J. Zawadzka, D. J. Jaroszynski, and Klaas Wynne, Phys. Rev. Lett. **84**, 1431 (2000).

[20] R. Ziolkowski, Phys. Rev. E **63**, 046604 (2001).

[21] A. M. Shaarawi and I. M. Besieris, J. Phys. A **33**, 8559 (2000).

[22] A. P. L. Barbero, H. E. Hernández-Figueroa, and E. Recami, Phys. Rev. E **62**, 8628 (2000).

[23] V. S. Olkhovsky, E. Recami, and G. Salesi, Europhys. Lett. **57**, 879 (2002).

[24] A. A. Stahlhofen, Phys. Rev. A **62**, 012112 (2000).

[25] A. Haibel, G. Nimtz, and A. A. Stahlhofen, Phys. Rev. E **63**, 047601 (2001).

[26] D. Mugnai, Opt. Commun. **188**, 17 (2001).

[27] A. M. Shaarawi, I. M. Besieris, A. M. Attiya, and E. El-Diwany, J. Acoust. Soc. Am. **107**, 70 (2000).

[28] W. C. Chew, *Waves and Fields in Inhomogeneous Media*, Series on Electromagnetic Waves (IEEE, New York, 1995).

[29] I. S. Gradshteyn and I. M. Ryzhik, *Tables of Integrals, Series and Products* (Academic, New York, 1965).

[30] A. M. Attiya, E. A. El-Diwany, A. M. Shaarawi, and I. M. Besieris, Prog. Electromagn. Res. **30**, 191 (2000).

[31] P. Saari, in *Time's Arrows, Quantum Measurement and Superluminal Behavior*, Scientific Monographs: Physics Sciences Series (CNR, Rome, 2001), p. 37.

[32] A. M. Shaarawi and I. M. Besieris, J. Phys. A **33**, 7227 (2000).

[33] A. M. Shaarawi and I. M. Besieris, J. Phys. A **33**, 7255 (2000).

[34] D. Mugnai, A. Ranfagni, and R. Ruggeri, Phys. Rev. Lett. **84**, 4830 (2000).

[35] W. A. Rodriguez, Jr. and J. Y. Lu, Found. Phys. **27**, 435 (1997).

[36] V. S. Barashenkov and W. A. Rodriguez Jr., NASA Conf. Publ. **113B**, 329 (1998).

[37] A. Dogariu, A. Kuzmich, H. Cao, and L. J. Wang, Opt. Express **8**, 344 (2001).

[38] E. Bolda, J. C. Garrison, and R. Y. Chiao, Phys. Rev. A **49**, 2938 (1994).

[39] K. McDonald, LANL archive, Report No. 0008013, 2000.